ACS OMEGA

http://pubs.acs.org/journal/acsodf
Article

Surface-Functionalized Magnetic Silica-Malachite Tricomposite (Fe−M−Si tricomposite): A Promising Adsorbent for the Removal of Cypermethrin

Published as a part of the ACS Omega virtual special issue "Magnetic Nanohybrids for Environmental Applications".

Syeda Noor Ul Ain, Muhammad Saqib Khan, Nadia Riaz,* Ajmal Khan,* Amna Sarwar, Asaad Khalid, Afnan Jan, Qaisar Mahmood,* and Ahmed Al-Harrasi*

Cite This: *ACS Omega* 2024, 9, 13803−13817

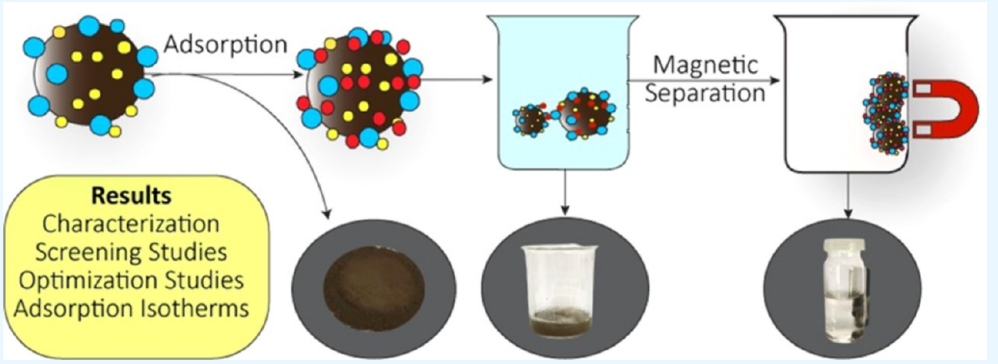

ABSTRACT: This study assessed the efficacy of adsorption for eliminating the agricultural pesticide cypermethrin (CP) from wastewater using various adsorbents: silica, malachite, and magnetite. Magnetic nanocomposites (NCs) (with varying amounts of Fe_3O_4 0.1, 0.25, 0.5, 1.0, and 1.5 wt/wt %) were synthesized, including Fe_3O_4 nanoparticles (NPs), bicomposites, and tricomposites, calcined at 300 and 500 °C, and then tested for CP removal. The study was conducted in two phases, with the objective of initially assessing how effectively each individual NP performed and then evaluating how effectively the NCs performed when used for the adsorption of CP. Notably, the Fe_3O_4−malachite combination exhibited superior CP removal, with the 0.25-Fe−M NC achieving the highest adsorption at 635.4 mg/g. This success was attributed to the large surface area, magnetic properties of Fe_3O_4, and adsorption capabilities of malachite. The Brunauer−Emmett−Teller (BET) isotherm analysis indicated that the NCs had potential applications in adsorption and separation processes. The scanning electron microscopy and transmission electron microscopy revealed the spherical, irregular shaped morphology of the synthesized NPs and NCs. However, the X-ray diffraction (XRD) pattern of surface functionalized materials such as surface functionalized malachite $[Cu_2CO_3(OH)_2]$ with Fe_3O_4 and SiO_2 may be complicated by the specific functionalization method used and the relative amounts and crystallographic orientations of each component. Therefore, careful interpretation and analysis of the XRD pattern, along with other techniques, are necessary for accurate identification and characterization of the functionalized material. The originality of this study lies in its comprehensive investigation of several adsorbents and NCs for CP removal at neutral pH. The innovation stems from the synergistic action of Fe_3O_4 and malachite, which results in improved CP removal due to their combined surface properties and magnetic characteristics. The application of magnetic NCs in adsorption and separation, as validated by BET isotherm analysis, highlights the potential breakthrough in addressing pesticide contamination.

1. INTRODUCTION

The most important component of life is water, and survival without it is impossible. The earth's crust has less fresh water, which is becoming contaminated as a result of improper waste disposal in streams and rivers. All pollutants, whether inorganic or organic, have an impact on the environment. The presence of hazardous metals at low concentrations can even cause a

Received: October 25, 2023
Revised: January 26, 2024
Accepted: February 7, 2024
Published: March 14, 2024

https://doi.org/10.1021/acsomega.3c08419
ACS Omega 2024, 9, 13803−13817

variety of diseases that are detrimental to living organisms.[1,2] Pollutants are mostly derived from three sources: sewage dumped into the river, industrial effluent discharged into the rivers, and runoff from agricultural land where chemical fertilizers, herbicides, insecticides, and manures are utilized.[3] In the last few decades, pesticides are found in water bodies as a result of rapid industrialization and extensive use in agricultural activities.[4] Pesticides are known as emerging organic compounds, and their presence in wastewater is increasing due to human activities.[5] Rapid food demand encourages pesticide usage in agricultural activities.[6] The overuse of chemical fertilizers and pesticides in modern agriculture practices has contaminated the environment, i.e., air, land, and water. As a result, a polluted environment has an adverse impact on human and nontargeted species in many ways.[7]

Cypermethrin (CP), a pyrethroid manufactured from pyrethrin (Figure S1), is a commonly used, efficient, and widely available pyrethroid. It is most commonly used in protecting cotton and soybean crops from pests. Unfortunately, its reckless misuse has serious negative consequences for the environment, especially for aquatic species.[8,9] It has been reported in water bodies along with the sediments as a result of runoff and erosion from farm areas.[10] In Southern Malawi, the concentration of CP reported in surface water was 8.115−15.460 mg/L. It was reported that a major fish killing in Rawal Lake (Pakistan) was due to carbaryl and CP pollution.[11] The concentration of CP reported in Rawal Lake was 0.2−18.8 μg/L.[12] CP has a detrimental effect on the central nervous system and triggers allergic reactions. Some reported human health effects are nausea, blurred vision, coma, and breathing problems.[10] Long-term CP exposure has been linked to chronic neurologic effects, immunosuppression, and mutagenic effects.[8]

There are some renowned methods for pesticide treatment in wastewater, such as physical, chemical, and biological. However, adsorption is a simple, efficient, and commonly used physical treatment method for the removal of organic and inorganic contaminants. Adsorption has been proven superior to various water reuse techniques in terms of cost, flexibility, simplicity, ease of operation, and insensitivity to harmful contaminants. Adsorption does not form any toxic byproducts. It is a surface phenomenon that is determined by the accessible sites, the porosity, and the surface area of the adsorbent, along with numerous types of interactions.[13] In adsorption, the adsorbent is used, and on its surface, the adsorbate (pollutant) is adsorbed and thus separated.[14] Organic pollutants are adsorbed on the adsorbent's surface by many forces. Pollutants and adsorbents can interact in a variety of ways, including hydrophobic interactions, van der waal's forces, electrostatic interactions, $\pi-\pi$ stacking interactions, and hydrogen bonding. These interacting forces are primarily in charge of adsorption, which assists in eliminating pollutants.[15]

Nanotechnology has the potential to improve current environmental technologies by introducing new materials with higher performance, resulting in lower energy and material use.[13,16] The term "nano" refers to the process of decreasing the size of the substance to the nanoscale, which causes significant changes in the material's properties. As the material's size reduces, the surface area increases.[17] Magnetic Iron oxide nanoparticles (NPs) (Fe_3O_4 NPs or magnetic nanoparticles (MNPs)) have gained consideration because of their special properties, e.g., magnetism, larger surface area, and simple separation technique.[18] MNPs have recently been investigated for their possible applications in dyes, pesticides, and heavy metal removal.[19]

Malachite is a bright green, dark green, and black-green secondary copper carbonate hydroxide (Cu_2 (CO_3) $(OH)_2$ mineral that has 57.48% Cu in its finest form. The formation of malachite is caused by the surface weathering of copper ore and is often not used for copper extraction due to limited resources and insufficient metallurgical recovery. Malachite is a mineral pigment used in paints and as a decorative ornamental stone.[20] It is also utilized to make copper compounds (CuO), catalysts in methanol synthesis, wood preservatives, and antimicrobial agent.[21] Malachite NPs (basic copper carbonate, $Cu_2(OH)_2CO_3$) have been used in various studies for dye adsorption.[22]

Bare Fe_3O_4 NPs have been most widely used among the magnetic adsorbents for different pesticides.[23] However, the shortcomings of using Fe_3O_4 NPs are their accumulation and lack of target specificity. The magnetism generates intrinsic instability due to agglomeration, resulting in large particles.[24] The surface of MNPs can be functionalized to overcome these limitations. For example, Fe_3O_4 supported on polystyrene,[4] graphene oxide,[25] graphene oxide-based silica-coated,[26] SiO_2,[27] and magnetic biochar[28] were used for Fe_3O_4 NPs functionalization as effective adsorbents. Some are reported along with their performance for various pesticides and other pollutants removal from wastewater in terms of adsorption capacity (Q_m, mg/g), contact time (C_T, min), working pH, and related isotherm models (L = Langmuir and F= Freundlich) used for experimental data fitness. These are summarized in Table S1.

Introducing Fe−M−Si tricomposite (TC), a magnetic silica−malachite TC that can adsorb CP. Unmodified MNPs have the advantage of being easy to recover, but they tend to aggregate and lack specificity. They also tend to cluster in water and oxidize in air. By modifying MNPs with materials such as malachite, SiO_2, and TiO_2 nanostructures, they can be stabilized. Fe−M−Si TC is synthesized using a coprecipitation-assisted wet impregnation method and shows high efficiency in adsorbing CP. The tricomposites were comprehensively characterized using Brunauer−Emmett−Teller (BET), Fourier transformed infrared spectroscopy (FTIR) spectroscopy, X-ray diffraction (XRD), scanning electron microscopy (SEM), and transmission electron microscopy (TEM) to understand its surface area, pore diameter, surface functional groups, crystallite size, diffraction patterns, and morphological characteristics. Fe−M−Si TC has the potential to be a magnetic nanocomposite (NC) adsorbent for the removal of pesticides from contaminated water. This study presents a novel approach to tackle CP contamination in water. Our surface-functionalized magnetic silica-malachite TC (Fe−M−Si TC) provides a constructive solution to the challenges faced by unmodified MNPs. By incorporating organic substances like malachite, SiO_2, and TiO_2 nanostructures, our modified composite addresses the limitations of unmodified MNPs, providing increased stability. Synthesized through coprecipitation-assisted wet impregnation, Fe−M−Si TC exhibits remarkable CP adsorption efficiency, validated through BET, FTIR, XRD, SEM, and TEM analysis. This TC has immense potential to eliminate pesticides from water or soil, making it a promising solution to environmental concerns.

2. MATERIALS AND METHODS

2.1. Synthesis of Magnetite (Fe), Malachite (M), Silica (SiO_2) NPs, Fe−M NCs (Fe−M-NC), and Magnetic Silica-

https://doi.org/10.1021/acsomega.3c08419
ACS Omega 2024, 9, 13803−13817

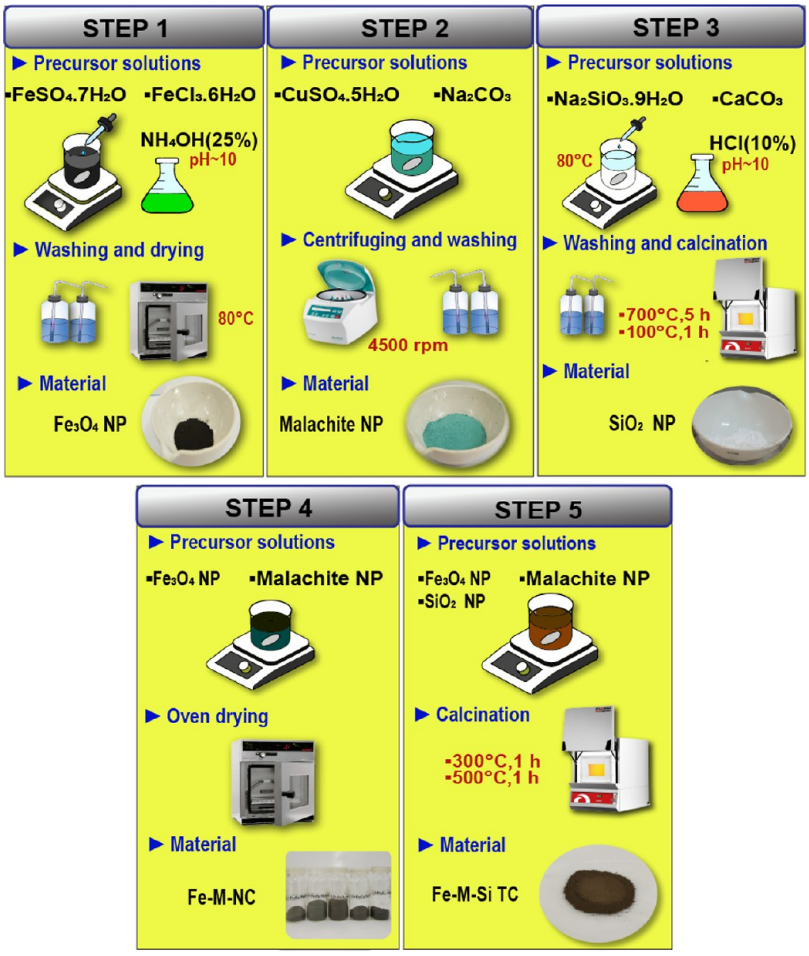

Figure 1. Synthesis of (step 1) Fe_3O_4 (step 2) Malachite (step 3) Silica ($SiO_{2)}$ NP (step 4) Fe−M bicomposite and (step 5) Fe−M−Si tricomposites. "Photograph courtesy of "Syeda Noor Ul Ain". Copyright 2023".

Malachite TC (Fe−M−Si TC). To synthesize MNP, composites, and tricomposites, a list of required chemicals and reagents, along with their cost, are listed in Supporting Information.

2.1.1. Synthesis of Fe_3O_4 NPs. The popular and effective chemical precipitation technique was employed to synthesize MNPs, as reported by Shah et al., (2018).[29] 2.1 g of ($FeSO_4$·$7H_2O$) and 3.1 g of ($FeCl_3$·$6H_2O$) were dissolved in 40 mL of distilled water separately. The solutions were mixed and heated up to 80 °C, accompanied by continuous stirring. Dropwise NH_4OH (25%) was added for the adjustment of the pH to 10 with constant stirring until the solution turned dark black. The solution was filtered, and then the NPs were washed thrice with ethanol and distilled water. MNPs were oven-dried at 80 °C overnight. The synthesized NP is shown in step 1, as shown in Figure 1.

2.1.2. Synthesis of Malachite NPs. The synthesis of malachite NPs was carried out following the procedure reported by Molchan et al., (2008).[30] 4.99 g of copper sulfate pentahydrate ($CuSO_4$·$5H_2O$) was dissolved in 50 mL of EG (ethylene glycol), and 2.75 g of Na_2CO_3 was dissolved in 12 mL of distilled water, followed by mixing in EG (50 mL). The solution of $CuSO_4$·$5H_2O$ was added to Na_2CO_3 dropwise along with continuous stirring, which resulted in a green particle-like suspension. Washing was carried out in two steps and centrifuged at a speed of 4500 rpm. The first washing involved three washings with ethanol, and the second washes was carried out with distilled water. Then the NPs were filtered and left to dry at room temperature. The synthesized NPs are shown in step 2, as shown in Figure 1.

2.1.3. Synthesis of Silica (SiO_2-NP) NPs. Sodium silicate (Na_2SiO_3·$9H_2O$) was used to synthesize SiO_2 NP, shown as step 3 in Figure 1. Within 1 h, sodium silicate was slowly added dropwise along with stirring to a nanosized calcium carbonate slurry, which was maintained at 80 °C using a water bath. The pH was adjusted by adding 10 wt % HCl solution (pH range = 9−10). 1/10 molar ratio SiO_2/$CaCO_3$ mixture was synthesized. After stirring for 2 h, the mixture was filtered, rinsed with distilled water and ethanol, and finally dried at 100 °C in an oven. Calcination at 700 °C for 5 h yielded $CaCO_3$−SiO_2 NPs core−shell composite. To completely extract $CaCO_3$, the composite of $CaCO_3$−SiO_2 was treated in 10 wt %, HCl for 12 h. The remaining gel was cleaned and washed with distilled water. Once the gel is rinsed, silica NPs are calcined at 100 °C for 1 h.[31]

2.1.4. Fe−M-NC. Using the WI method (wet impregnation), a series of Fe−M NCs with varying Fe_3O_4 (Fe-NP) loadings (0.1, 0.25, 0.5, 1.0, and 1.5 wt/wt %) were synthesized (as depicted as step 4 in Figure 1). Distilled water was used to dissolve different concentrations of Fe-NP. With the addition of M-NP as a substrate, the solution was repeatedly agitated to make a homogeneous solution. For 1 h, the slurry solution was constantly stirred. By keeping the solution in a water bath and continuously stirring it, the solution evaporated, resulting in a

https://doi.org/10.1021/acsomega.3c08419
ACS Omega 2024, 9, 13803−13817

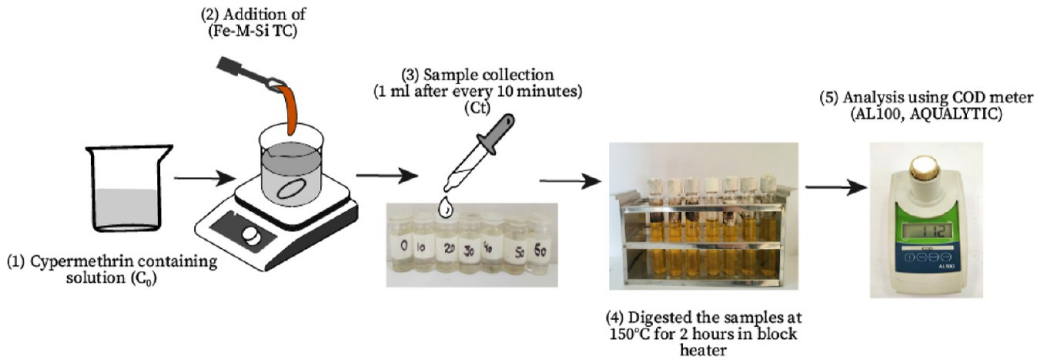

Figure 2. Process for batch adsorption experiment "Photograph courtesy of "Syeda Noor Ul Ain1". Copyright 2023".

thick slurry. The Fe−M NC was dried in the oven. The dried material was grinded and placed in a desiccator to be used later.[32,33]

2.1.5. Fe−M−Si tricomposite. The TC was synthesized using the coprecipitation-assisted wet-impregnation method with a Fe_3O_4 loading of 0.25 wt/wt %. First, Fe−M was mixed in distilled water until a homogeneous solution was formed. Then, silica dioxide (SiO_2) was added, and the solution was repeatedly agitated for 30 min. The resulting slurry solution was continuously stirred for another 30 min and transferred to a water bath to form a thick paste. The Fe−M−Si TC samples were then oven-dried and ground, as depicted as step 5 in Figure 1. Additionally, the samples were calcined at two different temperatures (300 and 500 °C) for 1 h.

2.2. Characterization. To understand the physicochemical properties of selected NP and NC, various characterization techniques were employed. The surface chemistry of the NC and NPs (in powder form) was analyzed using FTIR in the range of 500−4000 per cm. The BET surface area is a measure of the available surface area of a material that can come in contact with other substances, such as gases or liquids. In this study, the BET surface area of Fe_3O_4, SiO_2, malachite, and Fe_3O_4 loaded onto SiO_2 was determined using nitrogen adsorption−desorption isotherms at a very low temperature of −196 °C. The specific surface area was calculated using the BET equation, which is based on the adsorption of a gas on a solid surface. The slope of the linear portion of the BET equation gives the BET surface area of the material. The surface morphology of the samples was analyzed using SEM (JEOL JSM-6510LA) and transmission electron microscopy (TEM, JEM-1400), where microscopic images were taken at various resolutions using a JEOL JSM-6510LA scanning electron microscope (SEM with energy-dispersive X-ray spectroscopy (EDS) detectors to determine elemental composition) at the Electron Microscopy Unit, University of Nizwa, Nizwá, Oman. Phase analysis and crystallite size estimation were performed by XRD using a powder X-ray diffractometer (JDX-3532-JEOL, Japan) at the Material Resource Laboratory Peshawar, with Cu Kα radiation (λ = 1.5418 Å) and a 2 Theta range of 0−80°. The XRD spectra were analyzed using the Scherrer eq (eq 1 in S3) to calculate the crystallite size (ϕ) of the samples. In eq S1, 2θ represents the Bragg angle, K represents the shape factor, λ represents the X-ray wavelength, and β represents the full line width at the half-maximum height of the main intensity peak.

2.3. Batch Adsorption Experiments: Screening and Optimization. The study evaluated the adsorption capacity (Q_e, mg/g) of the synthesized MNPs, composites, and tricomposites for the removal of the pesticide CP following the protocol described previously.[34] The experimental parameters, including Fe_3O_4 loading, contact time, and calcination temperature (300, 500 °C), were varied to optimize the adsorption capacity. The best-performing NP was then further analyzed for its efficiency in removing the pesticide under different reaction parameters, such as contact time, adsorbent dose and initial pesticide concentration. Adsorption capacity and % removal efficiency of chemical oxygen demand (COD) was estimated to evaluate the adsorption efficiency of the NCs. Equations S1 and S2 were used for the calculations. The reaction samples were collected at regular intervals (1 mL every 10 min) and analyzed using a COD meter (AL100, AQUALYTIC). The experimental conditions for the adsorption studies included a neutral pH (7.2), a reaction duration of 1 h, and a reaction volume of 20 mL.

Adsorption studies for NCs, bicomposites, and tricomposites (illustrated in Figure 2) included assessing COD adsorption capacity and % removal efficiency. All trials were performed in triplicate. Equation S2 calculated COD adsorption capacity (Q_e, mg/g) for various time intervals (C_t), whereas eq 3 in Supporting Information (Table S3) was used to calculate % COD removal efficiency (mg/L).

Freundlich and Langmuir adsorption isotherms were used for data comparison to investigate CP adsorption behavior on different samples and comprehend the theoretical model.[35] The linear transformation of the Langmuir isotherm, shown in eq 4 (Table S3), indicates adsorption on a homogeneous surface.[36] The Freundlich isotherm (eq 5 in Table S3), on the other hand, is relevant to multilayer adsorption on heterogeneous surfaces and depicts nonideal and reversible adsorption.[37] All mathematical equations employed, as well as their appropriate units, are included in Supporting Information (Table S3).

2.4. Regeneration Experiments. Three cycles of adsorption and desorption studies were conducted for the NC regeneration. The best NCs were magnetically collected, washed multiple times with distilled water, and dried at 100 °C for 2 h after initially demonstrating high CP removal. Studies on batch adsorption and desorption were carried out later.

3. RESULTS AND DISCUSSION

3.1. Characterization. *3.1.1. FTIR Spectroscopy.* The FTIR spectrum of the composite material, Fe_3O_4−malachite loaded onto SiO_2, would exhibit various peaks that correspond to the vibrational modes of the different chemical bonds present in the material (Figure 3). The positions and intensities of these peaks would be influenced by the type

https://doi.org/10.1021/acsomega.3c08419
ACS Omega 2024, 9, 13803−13817

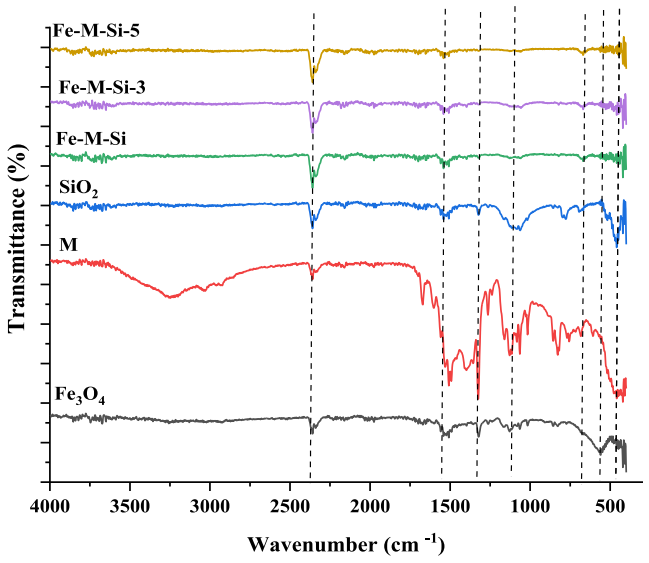

Figure 3. FTIR spectra of malachite and Fe_3O_4 NPs and related SiO_2 NCs (Raw and calcined at 300 and 500 °C).

and amount of chemical bonds present in the sample, as well as the analytical conditions. The peaks observed in the composite material (as shown in Figure 3) can be explained as follows: The Fe−O stretching vibrations of Fe_3O_4 could account for the peak observed at around 460−500 cm^{-1}.[38] The Si−O−Si stretching vibrations of SiO_2 could be responsible for the peak observed at around 1050−1150 cm^{-1}. The bending vibrations of CO_3 groups in the malachite mineral could explain the peak observed at around 1400−1500 cm^{-1}, while the stretching vibrations of C═O groups in the malachite mineral could account for the peak observed at around 1650−1750 cm^{-1}. Finally, the stretching vibrations of O−H groups in the composite material could be attributed to the peak observed at around 3000−3500 cm^{-1}.

3.1.2. Surface Area Analysis. This section examines the BET surface area and pore size of different materials, namely Fe_3O_4, SiO_2 (Fe−Si), malachite, and Fe_3O_4−SiO_2 NCs. BET analysis was utilized to determine the specific surface area of these materials, and the outcomes indicated that malachite possessed the highest surface area, whereas Fe−Si had the lowest surface area. The BET results demonstrated that Fe_3O_4 had a surface area of 17.507 m^2/g, SiO_2 had a BET surface area of 5.148 m^2/g, malachite had a BET surface area of 30.875 $m^2/$

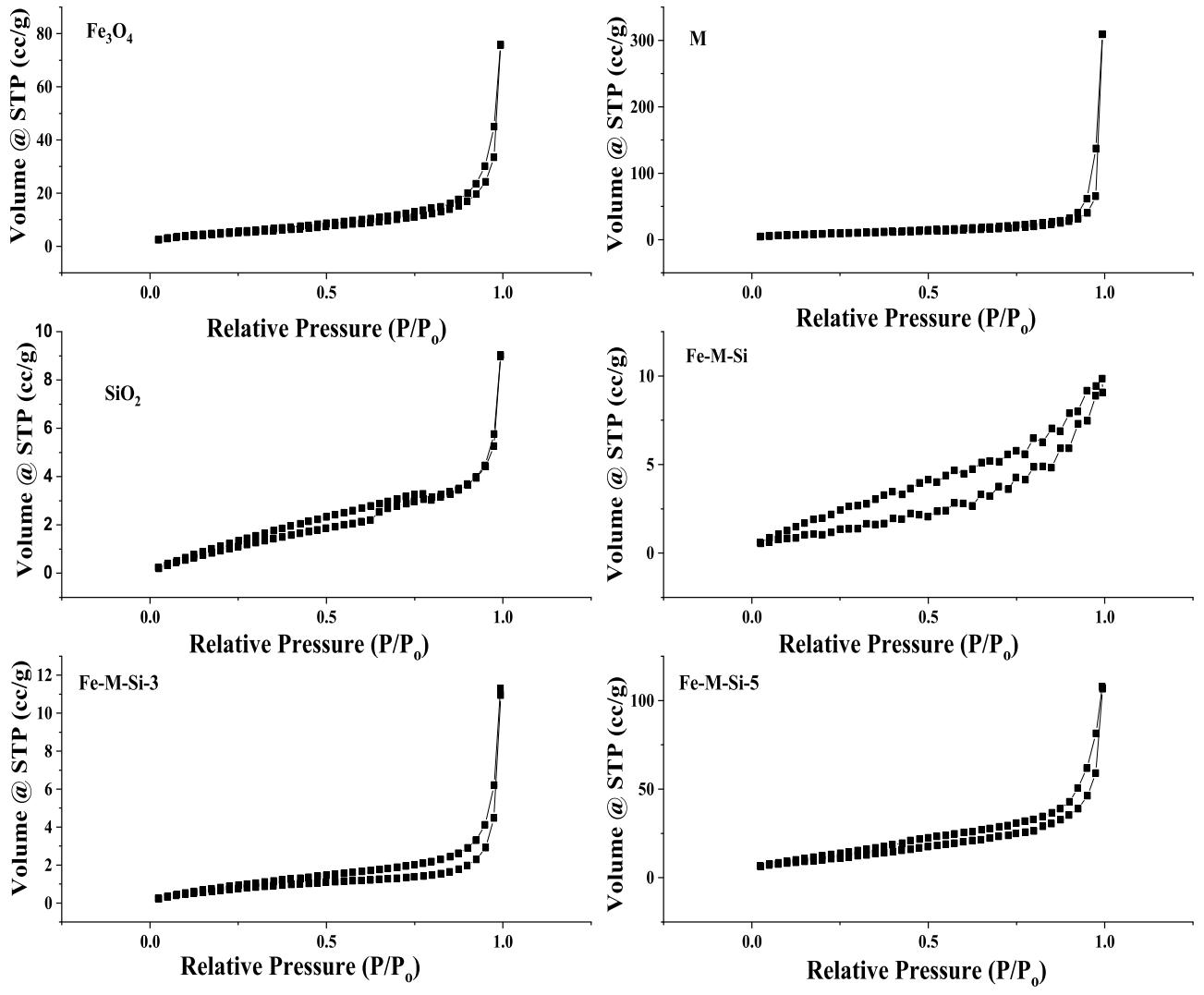

Figure 4. Nitrogen adsorption/desorption isotherm of NPs and related malachite NCs.

https://doi.org/10.1021/acsomega.3c08419
ACS Omega 2024, 9, 13803−13817

g, and Fe_3O_4 loaded onto SiO_2 had a BET surface area of 4.902 m^2/g. Additionally, BET surface areas of calcined Fe−M−Si 3 and Fe−M−Si-5 were reported as 2.903 and 8.849 m^2/g, respectively. Moreover, the NPs and related NCs exhibited higher pore sizes, with values of 1.8543, 1.5662, 1.8503, and 1.754 nm for Fe_3O_4, SiO_2, malachite, and Fe−Si, respectively. The pore sizes of calcined Fe−M−Si 3 and Fe−M−Si-5 were reported as 1.7491 and 1.7514 nm, respectively, which were slightly greater than the bare SiO_2 NP. This indicates that the NPs and related NCs possess more accessible surface areas for gas or liquid adsorption due to their higher pore sizes.

Furthermore, the results revealed that the addition of Fe_3O_4 to malachite led to a reduction in the specific surface area of the composite material. This could be due to the aggregation of Fe_3O_4 NPs on the surface of malachite, resulting in the formation of larger particles and a decrease in surface area. However, the pore size of the composite material remained similar to that of malachite, suggesting that the addition of Fe_3O_4 did not significantly affect the pore structure of the composite material. Therefore, while the Fe_3O_4−malachite NCs may still be effective for various organic pollutants and pesticide adsorption, the reduced specific surface area should be taken into account when designing applications for this material.[39−42]

According to the BET isotherm analysis, Fe−Si NCs exhibit a Type IV isotherm with a hysteresis loop, indicating the presence of mesopores in the material (Figure 4). The hysteresis loop may be attributed to the presence of slit-shaped pores or interparticle voids. At low relative pressures, the adsorption capacity increases rapidly and then gradually levels off as the pressure increases. The desorption process follows a different path, suggesting that it is slower than the adsorption process. The results suggest that Fe_3O_4−SiO_2 has a significant number of mesopores, which could make it useful for catalysis or adsorption applications.[43] In the case of malachite NPs, both SiO_2 and malachite-SiO_2-based Fe_3O_4 NCs exhibited higher adsorption capacities compared to bare malachite NPs. The BET isotherms of both NCs also exhibit hysteresis loops, indicating the presence of mesopores or macropores in the materials. The malachite-SiO_2 NC exhibited a Type H_2 hysteresis loop, while the malachite-Fe_3O_4 NC shows a Type H_3 hysteresis loop, indicating the presence of cylindrical and slit-like pores. These results suggest that the NCs have potential applications in adsorption and separation processes.

The discrepancy between low BET surface areas and high adsorption capacities suggests possible causes, including multilayer adsorption, in which several layers of adsorbate molecules may contribute to larger capacities even in the case of a low surface area. Adsorption may be enhanced through pore structure, particularly micropores, which BET is unable to entirely capture. Localized high-adsorption sites that are not reflected in the total surface area may be formed by surface heterogeneity. Adsorption may also be impacted by other variables, such as the experimental setting or particular interactions, that BET does not take into consideration. This variation indicates the intricacy of adsorption and the need for additional studies in order to fully comprehend its mechanics.

3.1.3. SEM−EDS and Transmission Electron Microscopy. The morphology of the synthesized NPs and NCs was examined using SEM and TEM. As illustrated in Figures 5 and 7, the SEM and TEM micrographs revealed that all Fe_3O_4-loaded NPs had an irregular shape, while both malachite and

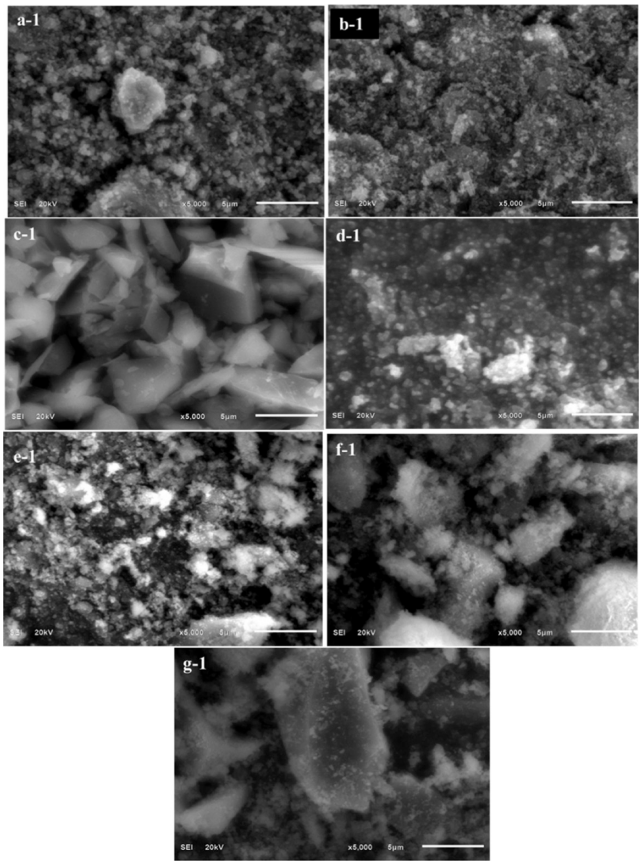

Figure 5. SEM micrograph of Fe_3O_4 NPs and related Malachite−Fe_3O_4 NCs. (a) Fe_3O_4, (b) malachite, (c) SiO_2, (d) TiO_2, (e) Fe−M−Si, (f) Fe−M−Si-3, and (g) Fe−M−Si-5.

Fe_3O_4−M NCs displayed a spherical and clustered morphology. This analysis provided insights into the physical characteristics and dimensions of the NPs and NCs, which are crucial in determining their properties and possible uses. SEM micrograph and EDS spectra of Fe_3O_4 NPs and related malachite−Fe_3O_4 NCs (Fe_3O_4, malachite, SiO_2, TiO_2, Fe−M−Si, Fe−M−Si-3, and Fe−M−Si-5) are presented in Figure 6. The SEM and EDS analyses of the Fe_3O_4/SiO_2@malachite NCs show significant peaks for O, malachite, Si, and Fe, confirming their presence. The high silica peak is attributed to the catalytic activity of Fe_3O_4 NPs, resulting in a high percentage of silica oxide in the composite. The EDS analysis confirms the homogeneous distribution of elements and the proper coverage of malachite on the Fe−Si particles, as evidenced by higher O and Fe element distributions. The lack of significant Fe_3O_4 peaks in the composite's EDS images could be due to signal interference with other materials in the composite or a low Fe_3O_4 concentration that falls below EDS detection limits. Furthermore, uneven coverage or dispersion within the composite could hinder Fe_3O_4 visibility in the examined locations.

TEM (as in Figure 7). was employed to analyze the microstructures of SiO_2, Fe_3O_4, malachite with 0.25 wt % Fe_3O_4, and malachite with 0.25 wt % Fe_3O_4 and SiO_2.

3.1.4. X-ray Diffraction. XRD is a powerful technique used to identify and characterize the crystalline structure of materials (as in Figure 8). The XRD pattern of Fe_3O_4 shows characteristic peaks (at specific 2θ angles of 27.19, 34.60, 35.92, and 62.77°) that correspond to the crystal planes of

https://doi.org/10.1021/acsomega.3c08419
ACS Omega 2024, 9, 13803−13817

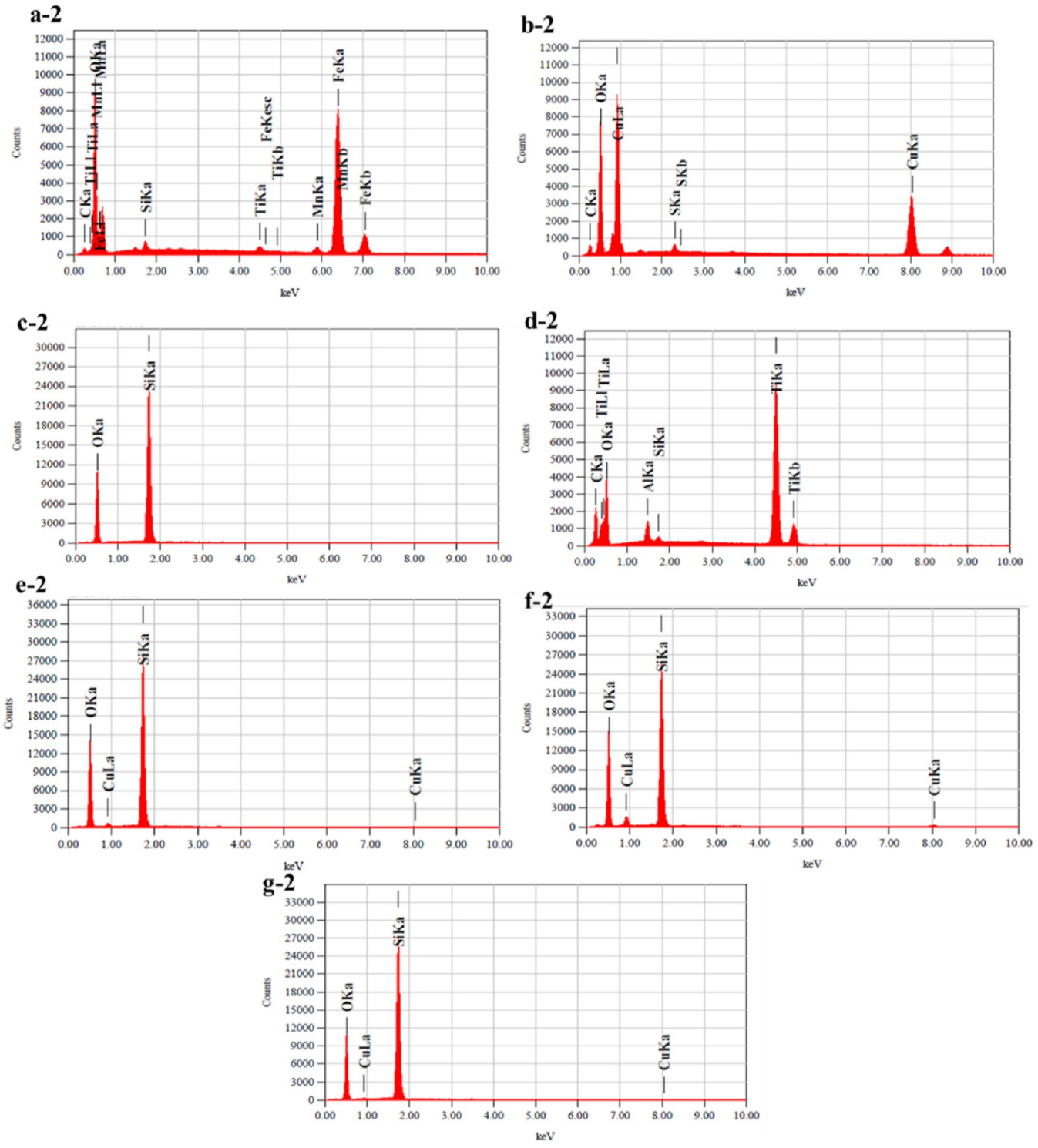

Figure 6. EDS spectra of Fe_3O_4 NPs and related Malachite−Fe_3O_4 NCs. (a) Fe_3O_4, (b) malachite, (c) SiO_2, (d) TiO_2, (e) Fe−M−Si, (f) Fe−M−Si-3, and (g) Fe−M−Si-5.

Fe_3O_4. The most intense peak at a 2θ angle of 27.19° corresponds to the (220) crystal plane, which is used to quantify Fe_3O_4. The (311) peak confirms the presence of Fe_3O_4, while the (222) peak is less intense but still useful. The (440) peak is weak but characteristic, and these four peaks together indicate the presence of Fe_3O_4 in the sample.

Malachite ($Cu_2CO_3(OH)_2$) also has characteristic peaks in XRD at specific 2θ angles of 15.8, 18.3, 21.5, 24.5, 27.5, 32.5, 36.0, 38.0, and 47.8°), corresponding to the (011), (020), (015), (110), (113), (006), (202), (116), and (018) crystallographic planes of malachite, respectively. The XRD pattern of malachite shows peaks at specific 2θ angles that correspond to the crystal planes of malachite. These peaks can be used to identify and characterize the presence of malachite in a sample.

SiO_2, which is the most common form of silicon dioxide, has characteristic peaks in XRD that correspond to the crystal planes of quartz. These peaks (20.92, 26.64, 36.59, and 39.59°

https://doi.org/10.1021/acsomega.3c08419
ACS Omega 2024, 9, 13803−13817

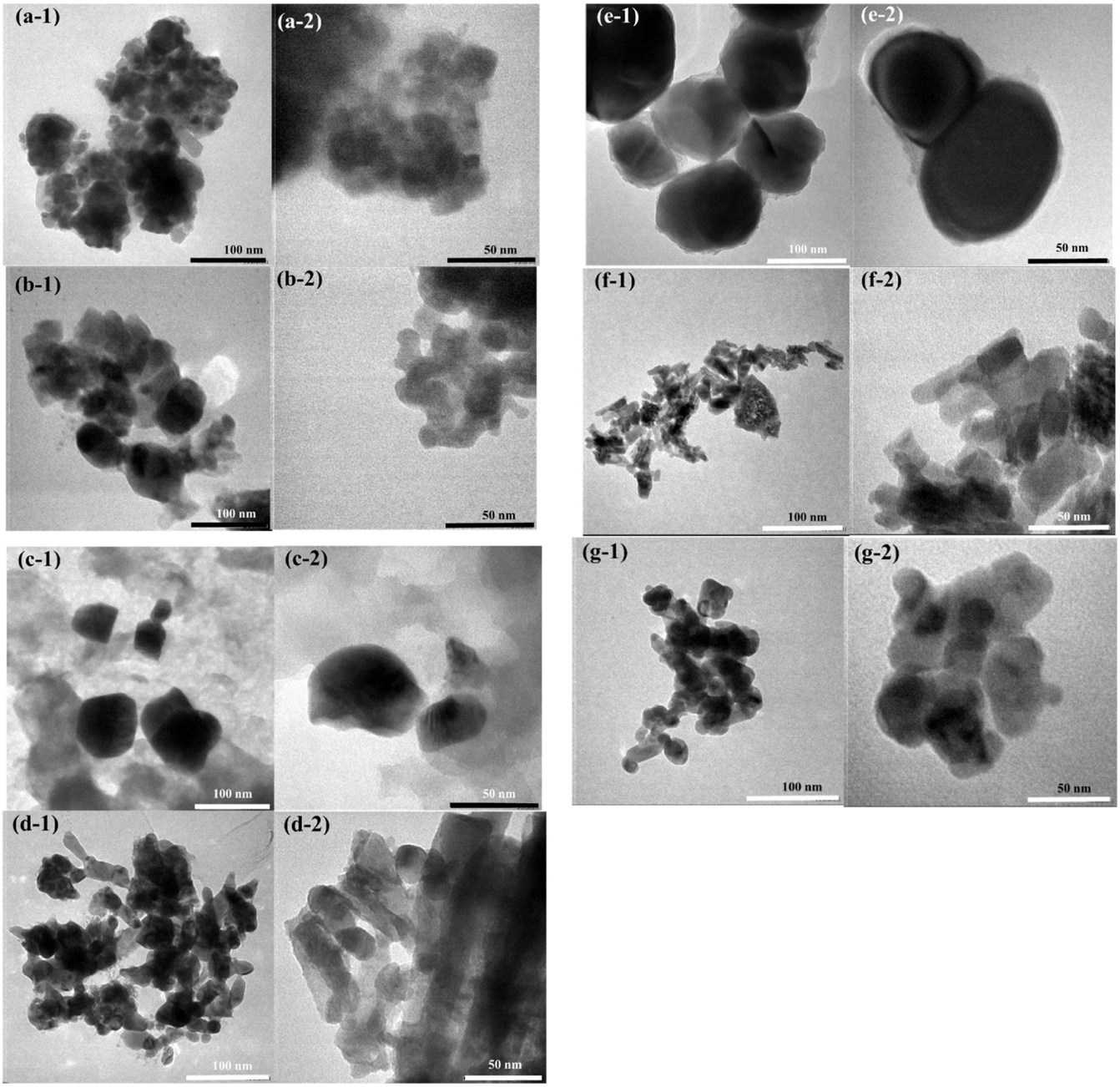

Figure 7. TEM micrograph of Fe_3O_4 NPs and related malachite−Fe_3O_4 NCs. (a) Fe_3O_4, (b) malachite, (c) SiO_2, (d) TiO_2, (e) Fe−M−Si, (f) Fe−M−Si-3, and (g) Fe−M−Si-5.

correspond to the (100), (101), (102), and (110) crystal planes of quartz, respectively) can be used to identify and characterize the presence of quartz in a sample. The peak at 45.81° corresponds to the (103) plane, while the peaks at 50.23, 55.02, and 59.806° correspond to the (200), (112), and (201) planes, respectively. Finally, the peak at 68.10° corresponds to the (202) plane. The characteristic peaks of SiO_2 (silicon dioxide) in XRD correspond to the crystal planes of the mineral quartz (α-quartz), which is the most common form of SiO_2. The characteristic XRD peaks for SiO_2 can be used to identify and characterize the presence of quartz in a sample. However, the peak intensity and position can be influenced by particle size, morphology, degree of crystallinity, and experimental conditions. Thus, careful analysis of XRD patterns and other characterization techniques may be necessary for accurate identification and characterization of SiO_2 materials.

The characteristic peaks for surface-functionalized malachite ($Cu_2CO_3(OH)_2$) with Fe_3O_4 and SiO_2 would depend on the specific functionalization method used and the relative amounts and crystallographic orientations of each component. The characteristic peaks for each individual component (Fe_3O_4, SiO_2, and malachite) described earlier would still be present, but their intensities, positions, and shapes could be influenced by the functionalization process. For example, if Fe_3O_4 NPs were functionalized onto the surface of malachite, the intensity of Fe_3O_4 peaks may be weaker than in a sample of pure Fe_3O_4 due to peak broadening caused by the small size of Fe_3O_4 NPs partially embedded in the malachite matrix. The SiO_2 matrix could also contribute to background signals and

https://doi.org/10.1021/acsomega.3c08419
ACS Omega 2024, 9, 13803−13817

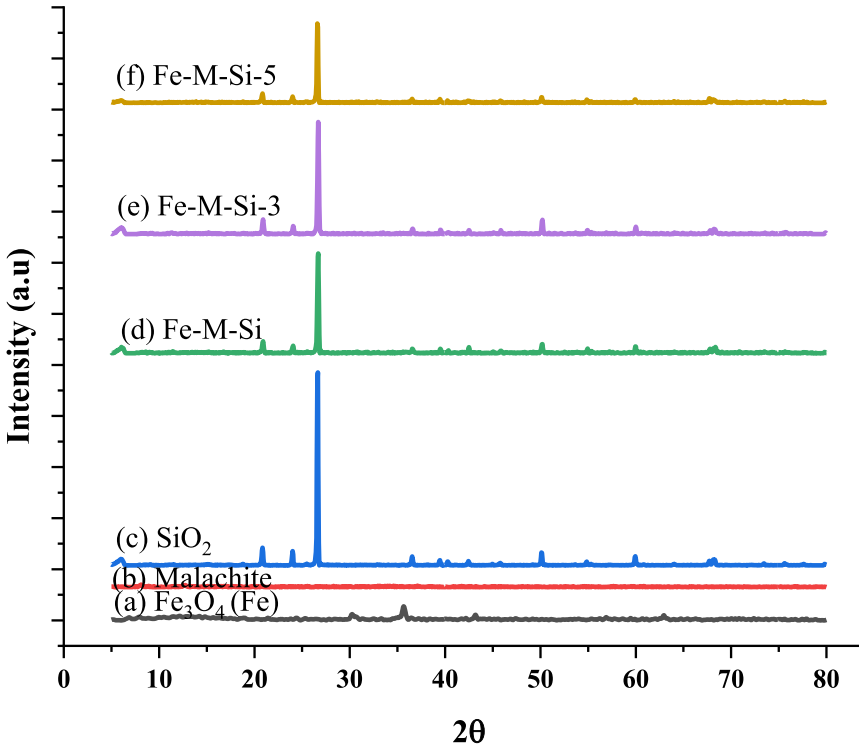

Figure 8. XRD pattern of Fe_3O_4 NPs and related Malachite−Fe_3O_4 NCs. (a) Fe_3O_4, (b) malachite, (c) SiO_2, (d) Fe−M−Si, (e) Fe−M−Si-3, and (f) Fe−M−Si-5.

lead to peak shifts, further complicating the XRD pattern. In addition, the surface functionalization process itself could introduce new peaks or shift the positions of existing peaks. Thus, careful interpretation and analysis of the XRD pattern and other techniques such as TEM or SEM may be necessary to accurately identify and characterize the functionalized material.

3.2. Screening Studies. The screening studies evaluated the adsorption efficiency of synthesized NPs, NCs, and tricomposites, and experiments were conducted in two stages. The study compared the performance of various NPs and NCs, including Fe_3O_4, malachite (M), silica (SiO_2), Fe−M−NCs, Fe−M−Ti, and Fe−M−Si TC. The first stage evaluated the performance of various concentrations of Fe_3O_4 coupled with malachite, while the second stage involved the synthesis of tricomposites using the optimal iron oxide loading and evaluation of their performance. To determine the optimal adsorption capability of malachite NCs with varying Fe_3O_4 loadings (0.1, 0.25, 0.5, 1.0, and 1.5 wt %), a study was conducted. The results indicated an unfavorable correlation between Fe_3O_4 loading and CP adsorption. This decline in COD adsorption was observed beyond a Fe−M ratio of 0.25 wt %. Despite this, the overall efficiency was still recorded at 90.13%, and the highest equitable adsorption was observed with 0.25-Fe−M, measuring 635.4 mg/g. Based on these findings, 0.25-Fe−M-NCs were selected for further research using varied adsorbent doses and initial CP concentrations. The adsorption recorded for the synthesized NCs 0.1Fe−M, 0.25Fe−M, 0.5Fe−M, 1.0Fe−M, and 1.5Fe−M were 527, 635.4, 591.5, 553, and 517 mg/g, respectively.

The results showed that when the Fe−M ratio exceeded 0.25 wt %, there was a negative correlation between Fe_3O_4 loading onto malachite for COD. The overall adsorption efficiency (as Q_e) ranged from 489 to 635.4 mg/g. As the Fe_3O_4 loading increased, the COD adsorption decreased. However, the overall efficiency improved, and the highest amount of equitable adsorption was observed with 0.25-Fe−M−Si at 635.4 mg/g. As a final response, 0.25-Fe−M−Si was selected for the synthesis of tricomposites. For various Fe_3O_4 amounts, the Q_e ranged from 489 to 635.4 mg/g, with a decrease in COD adsorption as the Fe_3O_4 loading increased. The 0.25-Fe−M−Si NC had the highest equitable adsorption and was selected for the synthesis of tricomposites.

3.3. Optimization Studies. *3.3.1. Effect of Coupling of SiO_2 and TiO_2 with Fe_3O_4-Malachite and Calcination Temperature.* In the second phase, malachite was coupled with magnetic Fe_3O_4, as well as semiconductors such as SiO_2 and TiO_2 to examine their effectiveness in adsorbing pesticides. The results of malachite bi and tricomposites (as in Figure 9a) indicated that Fe−M−Si TC exhibited the most effective performance in terms of adsorption capacity, surpassing both NPs and their NCs, with an adsorption capacity of 658.5 mg/g when the Fe_3O_4 concentration was 0.25, and it was calcined at 500 °C. Malachite, silica, and Fe_3O_4 NPs achieved maximum COD adsorption of 493.8, 549, and 489 mg/g, respectively. Furthermore, to evaluate whether the adsorption could be enhanced by coupling 0.25Fe−M NCs (which had a maximum adsorption of 635.4 mg/g in 1 h) with two distinct semiconductors, TiO_2 and SiO_2 NPs, experiments were conducted. However, the findings indicated that, compared to the NPs, Fe−M−Ti and Fe−M−Si TC showed improved performance, with adsorption capacities of 617.5 and 658.5 mg/g, respectively.

The addition of SiO_2 and TiO_2 can have a positive impact on the adsorption capacity and efficiency of Fe_3O_4/malachite (M) for removing contaminants from water or soil. SiO_2 can improve the stability and reusability of the adsorbent, making it more practical for large-scale applications.[22,40,42,44−48]

https://doi.org/10.1021/acsomega.3c08419
ACS Omega 2024, 9, 13803−13817

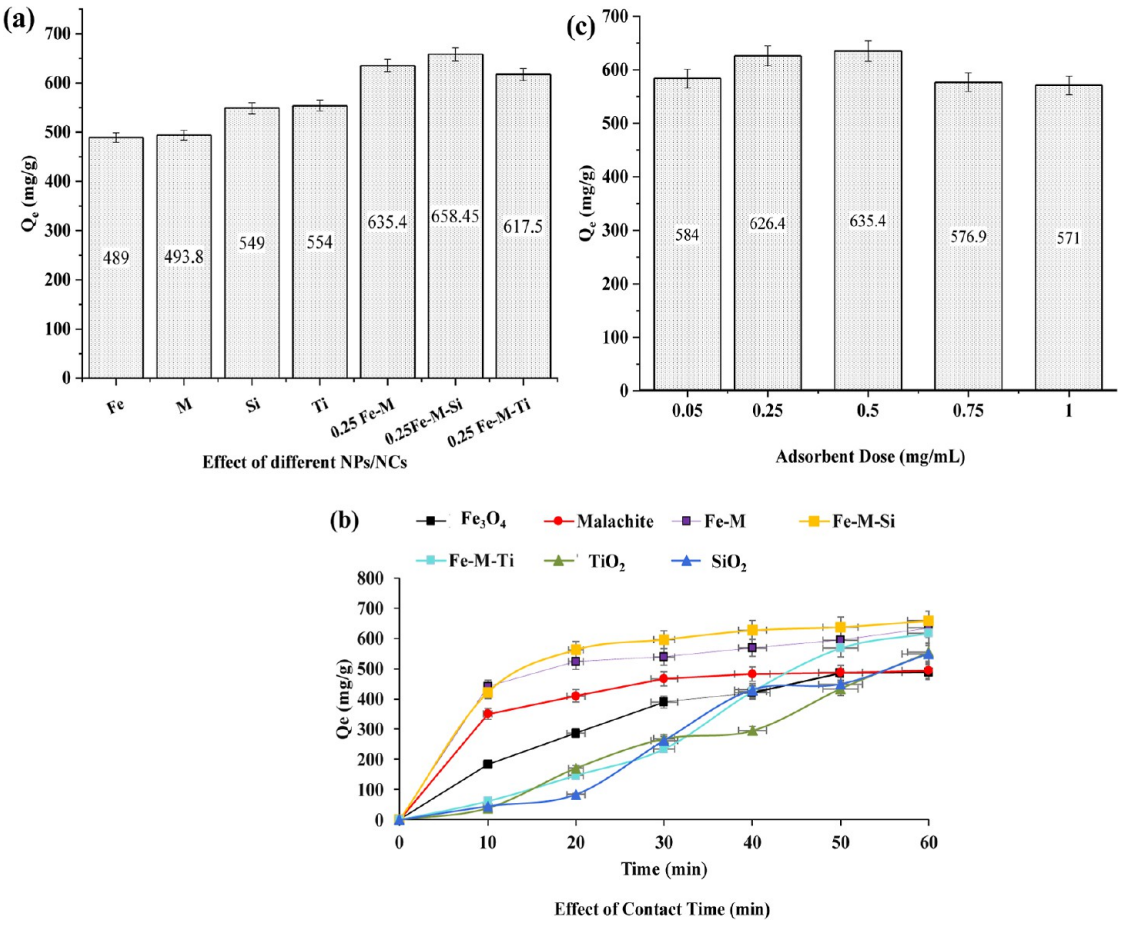

Figure 9. (a) Comparison of adsorption capacity of magnetic NPs and related NCs (mass = 1 mg/mL; CT = 60 min; pH 7.2). (b) Effect of CT (min) using NPs and related NCs (mass = 1 mg/mL; CT = 60 min; pH 7.2). (c) Effect of the adsorbent dose using 0.25 Fe−M NC (mass = 0.05−1 mg/mL; CT = 60 min; pH 7.2).

Studies have shown that the coupling of SiO_2 with Fe_3O_4 can significantly increase the adsorption capacity for organic contaminants such as phenol,[40] methylene blue,[41] and fluoride.[42] TiO_2 coupling with Fe_3O_4 can enhance the photocatalytic activity of the material, allowing for the degradation of contaminants like chlorpyrifos under light irradiation.[49] This approach has been explored for the removal of pesticides and dyes from contaminated water. In summary, the coupling of SiO_2 and TiO_2 with Fe_3O_4/malachite shows great potential for improving the efficiency and effectiveness of adsorption and photocatalytic processes for environmental remediation.

3.3.2. Effect of CT. Following the selection of the most appropriate 0.25-Fe−M−Si TC, which underwent calcination at 500 °C, a subsequent investigation was carried out to evaluate the effect of CT on COD adsorption. The study spanned over a duration of 60 min, with an initial concentration of CP (model pollutant) of 0.048 mM. The obtained results were graphed on an L-shaped graph for 0.25-Fe−M−Si TC, exhibiting the maximum adsorption for NP, their NC, and TC within the specified time frame, as illustrated in Figure 9b. A negligible rise in adsorption was recorded for NC, which might be attributed to the adsorbent's surface area and pore structure. It was observed that longer contact between the adsorbate and adsorbent caused an increase in adsorption.

The given data represents the effect of contact time (in minutes) on the performance of selected NPs (Fe_3O_4 and malachite) and their NCs (0.25-Fe−M, 0.25 Fe−M with TiO_2 and SiO_2) in terms of pesticide adsorption. The graph represents the concentration of the pesticide (in ppm) after a certain contact time with the NP. At the beginning (0 min), all NPs/NCs show no adsorption because the NPs have not yet been in contact with the pollutant. As the contact time increases, the concentration of the pesticide decreases, indicating that the NPs are effective at removing it from the solution. The NC 0.25-Fe−M has the lowest concentration of pesticide at each time point, suggesting that the combination of Fe and M NPs has a synergistic effect on pesticide adsorption. Moreover, the NC 0.25 Fe−M with TiO_2 and SiO_2 shows improved performance compared to 0.25-Fe−M, with even lower pesticide concentrations at each time point. This suggests that the addition of TiO_2 and SiO_2 has enhanced the pesticide adsorption capacity of the NC.[50,51] Overall, the data indicates that the selected NPs and their NCs are effective at removing pesticides from the solution, and the addition of TiO_2 and SiO_2 can further improve their performance.

3.3.3. Effect of Adsorbent Dose. This study investigated the impact of the dose of the adsorbate on pesticide adsorption using 0.25 Fe−M NC. The findings revealed that the adsorption capacity of pesticides increases as the dose of the adsorbate increases. The sample with a concentration of 0.5 mg/mL showed the highest adsorption capacity, with a Q_e

https://doi.org/10.1021/acsomega.3c08419
ACS Omega 2024, 9, 13803−13817

value of 635.4 mg/g. However, as the sample concentration increased, the percentage removal of pesticides decreased, indicating a declining trend in the adsorption efficiency. The data in Figure 9c further revealed that increasing the dose of NC led to an increase in the adsorption capacity of pesticides. Nonetheless, the Q_e values decreased from 584.0 to 571.0 mg/g, indicating that the adsorption capacity of the adsorbent decreased as the amount of NCs increased. The reduction in adsorption capacity was due to NP agglomeration that occurred when the dose of NCs exceeded a certain limit. This agglomeration reduced the available surface area for adsorption, leading to a decrease in the efficiency of the adsorption process. The reduction in surface area was attributed to excess NCs that blocked the available adsorption sites, thereby preventing pesticide molecules from being adsorbed. It is, therefore, essential to determine the optimum dose of NCs to achieve maximum adsorption capacity and efficiency.

3.3.4. Effect of Adsorbate Dose. At a neutral pH and over a contact period of 60 min, the process accelerated for the selected range of initial concentrations (0.048−0.432 mM), with the highest starting concentration leading to the fastest process. The initial concentrations studied were C1 (0.048 mM), C2 (0.14 mM), C3 (0.249 mM), C4 (0.348 mM), and C5 (0.432 mM). The adsorption capacity of 0.25-Fe−M−Si TC calcined at 500 °C increased from 635.4 to 1064.75 mg/g for the specified range of initial CP quantities, as depicted in Figure 10a. The data presented displays the results of adsorption experiments using Fe_3O_4 doped malachite as an adsorbent for the model pesticide, CP. The experiments were conducted at different initial concentrations of the pesticide, labeled as C1, C2, C3, C4, and C5. The results show that as the initial concentration of the pesticide increased from C1 to C5, the adsorption capacity of the adsorbent (Q_e) also increased. At the lowest concentration (C1), the adsorbent had an adsorption capacity of 635.4 mg/g, while at the highest concentration (C5), the adsorption capacity increased to 1064.75 mg/g. These findings suggest that Fe_3O_4-doped malachite is a promising adsorbent for the efficient removal of CP from aqueous solutions, with its adsorption capacity being influenced by the initial concentration of the pesticide. A decreasing trend for % COD removal (%) was observed as the concentration increased. An L-shaped curve was generated for the CP amount (Q_e) adsorbed at varied initial concentrations versus time. Figure 10 shows that different concentrations of the pesticide had significant results against the adsorption of a uniform dose of NPs (0.5 mg/mL). The results showed that as the initial concentration of CP increased, so did its adsorption capacity. Similar trends were reported in previous studies, such as the study on Hemoglobin/iron oxide composites (Hb/Fe_3O_4) for dye removal[S2] and the study by Essandoh and Garcia (2018)[S3] for the adsorption of pollutants. Both studies reported that the adsorption capability increased with increasing concentrations of the pollutant or dye, indicating that higher concentrations lead to more available adsorption sites on the adsorbent.

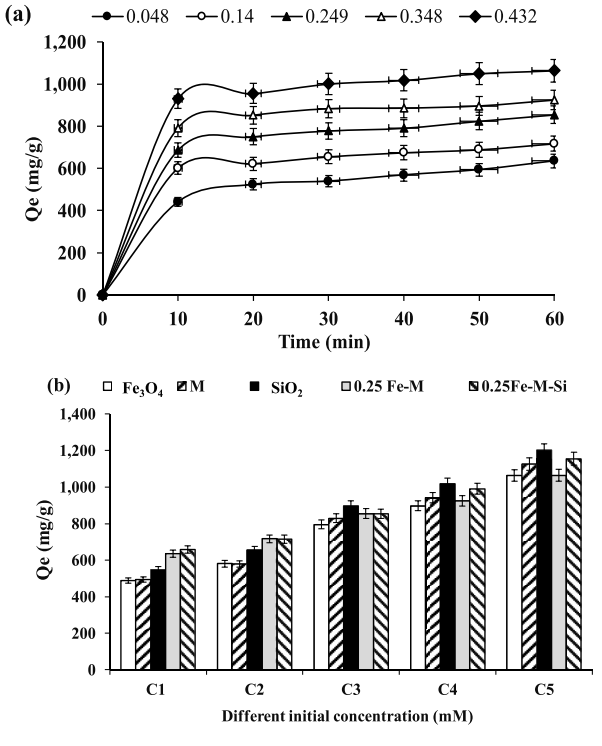

Figure 10. Quantity (Q_e) adsorbed at various initial CP concentrations (mM) vs (a) time using 0.25-Fe−M NC and (b) adsorption capacity of different NPs/NCs for CP adsorption at various concentrations.

Table 1 and Figure 10b presented display the mg/g adsorption capacity of various materials for the removal of COD at different concentrations of CP (0.048−0.432 mM, labeled as C1−C5). The materials evaluated for CP adsorption were Fe_3O_4, M (malachite), Si (silica), 0.25 Fe−M (Fe−malachite), 0.25 Fe−M−Si (Fe−malachite−silica), and two additional variations of 0.25 Fe−M−Si calcined at different temperatures (300 and 500 °C) named 0.25 Fe−M−Si-3 and 0.25 Fe−M−Si-5. The values in the table indicate the maximum COD adsorption capacity achieved by each material at various CP concentrations. Fe_3O_4, M, and Si all demonstrate different adsorption capacities at the lowest concentration (C1). For instance, Fe_3O_4 has an adsorption capacity of 489 mg/g, M has 493.8 mg/g, and Si has 549 mg/g. 0.25 Fe−M−Si material exhibits the highest COD adsorption capacity overall, with a maximum capacity of 658.45 mg/g at C1 (0.048 nM). Conversely, 0.25 Fe−M−Si-3 and 0.25 Fe−M−Si-5 show lower values than 0.25 Fe−M−Si, indicating that the addition of the third component could have led to a reduction in adsorption capacity after calcination. Table 1 also shows an increasing trend in adsorption capacity with an increase in the concentration of CP for some materials, such as 0.25 Fe−M and 0.25 Fe−M−Si.

Table 1. Adsorption Capacity of Different NPs/NCs for CP Adsorption at Various Concentrations

NPs/NCs	adsorption capacity (mg/g)				
	C1	C2	C3	C4	C5
Fe_3O_4	489.0	580.8	795.3	897.6	1064.2
malachite (M)	493.8	578.0	829.4	941.4	1125.2
SiO_2 (Si)	549.0	654.9	897.5	1017.8	1202.0
0.25Fe−M	635.4	717.4	855.4	924.6	1064.75
0.25Fe−M−Si	658.5	715.0	853.6	990.6	1156.0
0.25Fe−M−Si-3	445.8	556.2	772.6	705.1	679.25
0.25Fe−M−Si-5	412.5	800.0	657.5	592.5	546.75

3.4. Regeneration Experiments. The adsorbent's ability to regenerate is important for determining the material's cost-

https://doi.org/10.1021/acsomega.3c08419
ACS Omega 2024, 9, 13803−13817

effectiveness in the treatment of water. The Fe_3O_4−malachite combination exhibited superior CP removal, with the 0.25-Fe−M NC achieving the highest adsorption at 635.4 mg/g. Regeneration experiments were carried out in three cycles. The performance of NC was reduced after every cycle. The adsorption capacity, as shown in Figure 11, was reduced from

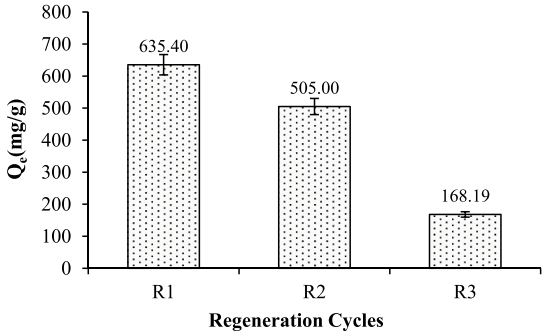

Figure 11. Regeneration of NCs for CP adsorption.

635.40 to 168.19 mg/g in the third regeneration cycle (R3). The % COD removal decreases to 23.86% in R3. A study reported that Malathion adsorption was carried out in five sequential cycles of desorption−adsorption with magnetic graphene oxide NC (MGO). With each new cycle, the MGO's adsorption capacity decreased (92.4−85.8%).[25]

The results of the regeneration studies indicate that the adsorbent has potential for partial reusability. Given the importance of water treatment, it is crucial to evaluate the adsorbent's potential industrial application and cost-effectiveness. In particular, the combination of Fe_3O_4−malachite has shown remarkable performance in removing CP, with a peak adsorption rate of 635.4 mg/g. However, as the adsorption process was repeated across three regeneration cycles, there was a noticeable decrease in the adsorbent's performance.

3.5. Adsorption Isotherms and Mechanism. The isotherm is focused on the interaction between the equilibrium adsorbate concentrations in the fluid phase and the equilibrium adsorption in the solid phase at a certain temperature. Langmuir (Figure 12a) and Freundlich isotherms (Figure 12b) were used to evaluate the processes in order to interpret experimental results and understand the equilibrium of adsorption at a neutral working pH. Based on the Langmuir adsorption isotherm data, SiO_2 exhibits the highest Q_m value of 3333.33 mg/g, indicating a greater adsorption capacity for CP compared to the other materials. Additionally, SiO_2 has the lowest K_{ads} value of 0.0000447 L/mg, suggesting stronger adsorption interactions. Fe_3O_4, on the other hand, has a lower Q_m value of 1666.6 mg/g and a slightly higher K_{ads} value of 0.00010446 L/mg compared to SiO_2. This indicates a lower adsorption capacity and weaker adsorption interactions for Fe_3O_4. Malachite displays an intermediate Q_m value of 1428.57 mg/g and a K_{ads} value of 0.00006622 L/mg, signifying a moderate adsorption capacity and interaction strength. When 0.25 wt % Fe_3O_4 is added to malachite, the Q_m value slightly decreases to 1111.11 mg/g while maintaining a similar K_{ads} value of 0.00004446 L/mg. This suggests a minor decrease in adsorption capacity without a significant change in adsorption interaction strength. However, coupling SiO_2 with malachite and 0.25 wt % Fe_3O_4 results in a composite with an increased Q_m value of 3333.33 mg/g and a higher K_{ads} value of 0.00027093 L/mg. This indicates a higher adsorption capacity

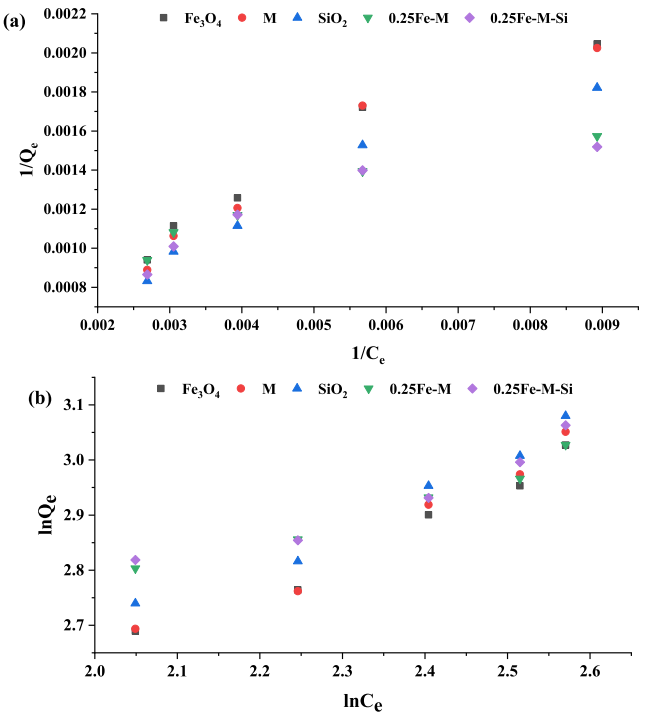

Figure 12. (a) Langmuir adsorption isotherm plot of $1/Q_e$ vs $1/C_e$ using different NPs/NCs and (b) Freundlich adsorption isotherm plot of ln Q_e vs ln C_e using different NPs/NCs for CP adsorption.

and stronger adsorption interactions compared to malachite alone or malachite with Fe_3O_4. In summary, the Langmuir adsorption isotherm data demonstrates that lower K_{ads} values correspond to weaker adsorption interactions and potentially lower adsorption efficiency. SiO_2 exhibits the highest adsorption capacity and relatively stronger interactions, followed by malachite, malachite with 0.25 wt % Fe_3O_4 and Fe_3O_4 alone. The addition of SiO_2 to malachite with Fe_3O_4 enhances both the adsorption capacity and interaction strength.

Comparing Langmuir and Freundlich adsorption isotherm data (Table 2) for SiO_2, Fe_3O_4, malachite with 0.25 wt % Fe_3O_4, and malachite with 0.25 wt % Fe_3O_4 and SiO_2 reveals distinct adsorption behaviors. Langmuir adsorption isotherm data for SiO_2 demonstrates the highest Q_m (maximum adsorption capacity) of 3333.3333 mg/g, followed by malachite (1428.5714 mg/g), 0.25Fe−M−Si (3333.3333 mg/g), 0.25Fe−M (1111.1111 mg/g), and Fe_3O_4 (1666.6667 mg/g). In case of Freundlich Isotherm, malachite exhibits the highest KF (adsorption capacity) of 5.9269 mg/g, followed by SiO_2 (3.4480 mg/g), Fe_3O_4 (3.8706 mg/g), 0.25Fe−M−Si (1.6916 mg/g), and 0.25Fe−M (1.6916 mg/g). Comparing the two isotherms, SiO_2 consistently displays high adsorption capacity, while malachite demonstrates the highest overall capacity. Fe_3O_4 exhibits lower capacity but relatively strong adsorption. The inclusion of Fe_3O_4 decreases capacity, yet the addition of SiO_2 counteracts this reduction, leading to comparable capacity. In conclusion, Langmuir and Freundlich isotherms offer complementary insights into the adsorption characteristics of SiO_2, Fe_3O_4, malachite with 0.25 wt % Fe_3O_4, and malachite with 0.25 wt % Fe_3O_4 and SiO_2, emphasizing differences in adsorption behavior and capacity.

The adsorption process of the Fe−M−Si TC adsorbent results in the formation of a layer of CP. The adsorption

https://doi.org/10.1021/acsomega.3c08419
ACS Omega 2024, 9, 13803−13817

Table 2. Langmuir and Freundlich Adsorption Isotherm Data

NPs/NCs	Langmuir			Freundlich		
	Q_m (mg/g)	K_{ads} (L/mg)	R^2	K_F	$1/n$	R^2
Fe_3O_4	1666.6667	0.0001	0.9484	3.8706	0.6421	0.9489
M	1428.5714	0.0001	0.9576	5.9269	0.4888	0.9743
SiO_2	3333.3333	0.0000	0.9920	3.4480	0.7503	0.9962
0.25Fe−M	1111.1111	0.0000	0.9303	1.6916	0.8003	0.9666
0.25Fe−M−Si	3333.3333	0.0003	0.9633	1.6916	0.8003	0.9666

process can be divided into three essential steps: the transfer of the pesticide from the solution to the surface of the TC, the binding of the pesticide onto the solid surface of the TC, and the movement of the pesticide within the particles of the TC. The interaction between organic pollutants and the adsorbent involves a variety of mechanisms, including hydrogen bonding, $\pi-\pi$ stacking, electrostatic forces, hydrophobic forces, and van der Waals forces. Charged pollutants tend to attach to adsorbents with opposite charges due to electrostatic attraction, which contributes to the removal of organic pollutants from wastewater. The adsorption process and subsequent removal of pollutants are largely governed by the combined forces mentioned above, which are influenced by the specific properties of the material.

The literature features materials with remarkable adsorption capacities for diverse contaminants, like dyes, pesticides, pharmaceuticals, and metals. Different superadsorbents have demonstrated high adsorption capacities for specific contaminants. For example, Beigi et al. (2023)[54] synthesized a magnetic pectin hydrogel@Fe_3O_4-bentonite NC with exceptional adsorption capacities of 909.091 mg/g for crystal violet and 833.333 mg/g for chlorpyrifos (CPF). Ohale et al. (2023)[55] highlighted magnesium oxide/chitosan/graphene oxide and graphene oxide/metal organic framework composites with impressive Norfloxacin adsorption capacities of 1114.8 and 1000 mg/g, respectively. Liao and Wang. (2018) developed Cu_2O SPs microspheres with a remarkable adsorption capacity of 7627 mg/g for amaranth removal, while Ghanbari and Ghafuri. (2023)[56] reported a double hydroxide composite with a 1000 mg/g adsorption capacity for diazinon removal. Additionally, Dat et al. (2018) demonstrated a magnetic composite for adsorbing uranium(VI) with a capacity of 2430 mg/g. Beyki et al. (2018)[57] synthesized magnetic NC that effectively removed methylene blue with a capacity of 7089 mg/g. These studies highlight the impressive adsorption capabilities of various NCs and materials for different contaminants, opening avenues for efficient water and wastewater treatment. The table with detailed parameters is presented in showcases different materials and NCs with specific high adsorption capacities for various contaminants.

4. CONCLUSIONS

Fe_3O_4 NP, their bicomposites, and TC have been successfully synthesized using the coprecipitation-assisted wet impregnation method and used as a magnetic NC for the efficient removal of CP (model pesticide) from wastewater. During one hour of batch reaction, the synthesized TC significantly outperforms the NP and NC for CP adsorption at neutral reaction pH. In conclusion, the study showed that surface functionalized malachite with Fe_3O_4 is a promising adsorbent for removing CP from contaminated water. The highest adsorption was observed with 0.25-Fe−M at 635.4 mg/g, which was further investigated in the second stage of the study. SiO_2 exhibits high adsorption capacity and weaker interactions, while malachite has the highest capacity. Fe_3O_4 has lower capacity but stronger interactions. The addition of Fe_3O_4 reduces capacity, but SiO_2 compensates for it, resulting in comparable capacity. Overall, SiO_2 and malachite have distinct adsorption characteristics, and the isotherms provide complementary insights into their behavior. The synthesized NCs were found to be effective for adsorption and separation processes, with Fe−Si NCs exhibiting mesoporous properties with cylindrical and slit-like pores. In summary, the characteristic XRD peaks for Fe_3O_4, malachite ($Cu_2CO_3(OH)_2$), and SiO_2 have been described, but the specific peaks for a surface-functionalized material would depend on the functionalization method and the relative amounts and crystallographic orientations of each component. Careful interpretation and analysis of the XRD pattern and other characterization techniques, such as TEM or SEM, may be necessary to accurately identify and characterize the functionalized material. These results suggest that the synthesized NCs have the potential for developing efficient and effective adsorption and separation processes for pollutant removal from contaminated water or soil. The discrepancy between low BET surface areas and high adsorption capacities suggests possibilities such as multilayer adsorption, pore structures unmeasured by BET (e.g., micropores), and surface diversity-induced localized high adsorption sites. Other factors, like experimental conditions and specific interactions that BET cannot capture, may also influence adsorption. The difference between the two highlights adsorption's intricacy, requiring additional research to fully grasp its mechanisms.

■ ASSOCIATED CONTENT

Supporting Information

The Supporting Information is available free of charge at https://pubs.acs.org/doi/10.1021/acsomega.3c08419.

MNPs for the removal of pesticides and other pollutants from wastewater; list of chemicals and materials used with an estimated cost; mathematical equations and related information; structure of CP (Sharma et al., 2018); and NCs with remarkable adsorption capacities (PDF)

■ AUTHOR INFORMATION

Corresponding Authors

Nadia Riaz − *Department of Environmental Sciences, COMSATS University Islamabad, Abbottabad 22060, Pakistan;* orcid.org/0000-0002-0931-1089; Email: nadiariazz@gmail.com

Ajmal Khan − *Natural and Medical Sciences Research Center, University of Nizwa, Nizwa 616, Sultanate of Oman;* Email: ajmalkhan@unizwa.edu.om

https://doi.org/10.1021/acsomega.3c08419
ACS Omega 2024, 9, 13803−13817

Qaisar Mahmood − *Department of Environmental Sciences, COMSATS University Islamabad, Abbottabad 22060, Pakistan; Department of Biology, College of Science, University of Bahrain, Sakhir 32038, Bahrain*; Email: drqaisar@cuiatd.edu.pk

Ahmed Al-Harrasi − *Natural and Medical Sciences Research Center, University of Nizwa, Nizwa 616, Sultanate of Oman*; orcid.org/0000-0002-0815-5942; Email: aharrasi@unizwa.edu.om

Authors

Syeda Noor Ul Ain − *Department of Environmental Sciences, COMSATS University Islamabad, Abbottabad 22060, Pakistan*

Muhammad Saqib Khan − *Department of Environmental Sciences, COMSATS University Islamabad, Abbottabad 22060, Pakistan; Department of Biomedical Sciences, Pak-Austria Fachhochschule Institute of Applied Sciences and Technology, Haripur 22621 Khyber Pakhtunkhwa, Pakistan*; orcid.org/0000-0002-0897-7436

Amna Sarwar − *Department of Environmental Sciences, COMSATS University Islamabad, Abbottabad 22060, Pakistan*

Asaad Khalid − *Substance Abuse and Toxicology Research Center, Jazan University, Jazan 45142, Saudi Arabia*

Afnan Jan − *Department of Pharmacognosy, Faculty of Pharmacy, Umm Al-Qura University, Makkah 21955, Saudi Arabia*

Complete contact information is available at: https://pubs.acs.org/10.1021/acsomega.3c08419

Notes

The authors declare no competing financial interest.

■ ACKNOWLEDGMENTS

This study was funded by the Deputyship for Research and Innovation, Ministry of Education, Saudi Arabia (project number ISP23-81).

■ REFERENCES

(1) Santhosh, C.; Velmurugan, V.; Jacob, G.; Jeong, S. K.; Grace, A. N.; Bhatnagar, A. Role of nanomaterials in water treatment applications: a review. *Chem. Eng. J.* **2016**, *306*, 1116−1137.

(2) Ahsan, W.; Al Bratty, M.; Alhazmi, H. A.; Attafi, I. M.; Khardali, I. A.; Abdelwahab, S. I. Determination of trace metal concentrations in different parts of the khat varieties (Catha edulis) using inductively coupled plasma-mass spectroscopy technique and their human exposure assessment. *Phcog. Mag.* **2019**, *15* (63), 449−458.

(3) Dwivedi, A. K. Researches in water pollution: A review. *Int. Res. J. Nat. Appl. Sci.* **2017**, *4* (1), 118−142.

(4) Rani, M.; Shanker, U. Degradation of traditional and new emerging pesticides in water by nanomaterials: recent trends and future recommendations. *Int. J. Environ. Sci. Technol.* **2018**, *15* (6), 1347−1380.

(5) El-Said, W. A.; El-Khouly, M. E.; Ali, M. H.; Rashad, R. T.; Elshehy, E. A.; Al-Bogami, A. S. Synthesis of mesoporous silica-polymer composite for the chloridazon pesticide removal from aqueous media. *J. Environ. Chem. Eng.* **2018**, *6* (2), 2214−2221.

(6) Bilal, M.; Iqbal, H. M.; Barceló, D. Persistence of pesticides-based contaminants in the environment and their effective degradation using laccase-assisted biocatalytic systems. *Sci. Total Environ.* **2019**, *695*, 133896.

(7) Liu, L.; Bilal, M.; Duan, X.; Iqbal, H. M. Mitigation of environmental pollution by genetically engineered bacteria—Current challenges and future perspectives. *Sci. Total Environ.* **2019**, *667*, 444−454.

(8) Ullah, S.; Zuberi, A.; Alagawany, M.; Farag, M. R.; Dadar, M.; Karthik, K.; Tiwari, R.; Dhama, K.; Iqbal, H. M. Cypermethrin induced toxicities in fish and adverse health outcomes: its prevention and control measure adaptation. *J. Environ. Manage.* **2018**, *206*, 863−871.

(9) Hussain, S.; Jali, A. M.; Alshahrani, S.; Khairat, K. H.; Siddiqui, R.; Alam, M. I.; Ali, R.; Mohammed, M.; Khan, A.; Al Shahi, H.; et al. Hepatoprotective and antioxidant effects of nanopiperine against Cypermethrin via mitigation of oxidative stress, inflammations and gene expression using qRT-PCR. *Int. J. Mol. Sci.* **2023**, *24* (20), 15361.

(10) Akbar, S.; Sultan, S.; Kertesz, M. Determination of cypermethrin degradation potential of soil bacteria along with plant growth-promoting characteristics. *Curr. Microbiol.* **2015**, *70* (1), 75−84.

(11) Kanyika-Mbewe, C.; Thole, B.; Makwinja, R.; Kaonga, C. C. Monitoring of carbaryl and cypermethrin concentrations in water and soil in Southern Malawi. *Environ. Monit. Assess.* **2020**, *192* (9), 595.

(12) Khan, M. I.; Shoukat, M. A.; Cheema, S. A.; Arif, H. N.; Niazi, N. K.; Azam, M.; Bashir, S.; Ashraf, I.; Qadri, R. Use, Contamination And Exposure Of Pesticides In Pakistan: A Review. *Pakistan J. Agric. Sci.* **2020**, *57* (1), 131−149.

(13) Taghizade Firozjaee, T.; Mehrdadi, N.; Baghdadi, M.; Nabi Bidhendi, G. R. Application of nanotechnology in pesticides removal from aqueous solutions-a review. *Int. J. Nanosci. Nanotechnol.* **2018**, *14* (1), 43−56.

(14) Ambaye, T.; Vaccari, M.; van Hullebusch, E. D.; Amrane, A.; Rtimi, S. Mechanisms and adsorption capacities of biochar for the removal of organic and inorganic pollutants from industrial wastewater. *Int. J. Environ. Sci. Technol.* **2021**, *18* (10), 3273−3294.

(15) Saxena, R.; Saxena, M.; Lochab, A. Recent progress in nanomaterials for adsorptive removal of organic contaminants from wastewater. *ChemistrySelect* **2020**, *5* (1), 335−353.

(16) Khan, Y.; Sadia, H.; Ali Shah, S. Z.; Khan, M. N.; Shah, A. A.; Ullah, N.; Ullah, M. F.; Bibi, H.; Bafakeeh, O. T.; Khedher, N. B.; et al. Classification, synthetic, and characterization approaches to nanoparticles, and their applications in various fields of nanotechnology: A review. *Catalysts* **2022**, *12* (11), 1386.

(17) Ealia, S. A. M.; Saravanakumar, M. In A review on the classification, characterisation, synthesis of nanoparticles and their application; *IOP Conference Series: Materials Science and Engineering*, IOP Publishing, 2017; p 032019.

(18) Ali, A.; Zafar, H.; Zia, M.; ul Haq, I.; Phull, A. R.; Ali, J. S.; Hussain, A. Synthesis, characterization, applications, and challenges of iron oxide nanoparticles. *Nanotechnol. Sci. Appl.* **2016**, *9*, 49−67.

(19) Sharma, M.; Kalita, P.; Senapati, K. K.; Garg, A. Study on magnetic materials for removal of water pollutants. *Emerging Pollutants-Some Strategies for the Quality Preservation of Our Environment*; InTech, 2018; pp 61−78..

(20) Haldar, S. K. *Introduction to mineralogy and petrology*; Elsevier, 2020.

(21) Srivastava, V.; Sharma, Y.; Sillanpää, M. Response surface methodological approach for the optimization of adsorption process in the removal of Cr (VI) ions by Cu_2 $(OH)_2CO_3$ nanoparticles. *Appl. Surf. Sci.* **2015**, *326*, 257−270.

(22) Saikia, J.; Sikdar, Y.; Saha, B.; Das, G. Malachite nanoparticle: a potent surface for the adsorption of xanthene dyes. *J. Environ. Chem. Eng.* **2013**, *1* (4), 1166−1173.

(23) Targhoo, A.; Amiri, A.; Baghayeri, M. Magnetic nanoparticles coated with poly (p-phenylenediamine-co-thiophene) as a sorbent for preconcentration of organophosphorus pesticides. *Microchim. Acta* **2018**, *185* (1), 15.

(24) Hernández-Hernández, A. A.; Aguirre-Álvarez, G.; Cariño-Cortés, R.; Mendoza-Huizar, L. H.; Jiménez-Alvarado, R. Iron oxide nanoparticles: synthesis, functionalization, and applications in diagnosis and treatment of cancer. *Chem. Pap.* **2020**, *74*, 3809−3824.

(25) Kalantary, R. R.; Azari, A.; Esrafili, A.; Yaghmaeian, K.; Moradi, M.; Sharafi, K. The survey of Malathion removal using magnetic graphene oxide nanocomposite as a novel adsorbent: thermodynamics, isotherms, and kinetic study. *Desalination Water Treat.* **2016**, *57* (58), 28460−28473.
(26) Nnadozie, E. C.; Ajibade, P. A. Multifunctional Magnetic Oxide Nanoparticle (MNP) Core-Shell: Review of Synthesis, Structural Studies and Application for Wastewater Treatment. *Molecules* **2020**, *25* (18), 4110.
(27) Shamsizadeh, Z.; Ehrampoush, M. H.; Dehghani Firouzabadi, Z.; Jasemi Zad, T.; Molavi, F.; Ebrahimi, A. A.; Kamranifar, M. Fe_3O_4@ SiO_2 magnetic nanocomposites as adsorbents for removal of diazinon from aqueous solution: isotherm and kinetic study. *Pigm. Resin Technol.* **2020**, *49*, 457−464.
(28) Mojiri, A.; Zhou, J. L.; Robinson, B.; Ohashi, A.; Ozaki, N.; Kindaichi, T.; Farraji, H.; Vakili, M. Pesticides in aquatic environments and their removal by adsorption methods. *Chemosphere* **2020**, *253*, 126646.
(29) Shah, K. H.; Ali, S.; Shah, F.; Waseem, M.; Ismail, B.; Khan, R. A.; Khan, A. M.; Khan, A. R. Magnetic oxide nanoparticles (Fe_3O_4) impregnated bentonite clay as a potential adsorbent for Cr (III) adsorption. *Mater. Res. Express* **2018**, *5* (9), 096102.
(30) Molchan, I.; Thompson, G.; Skeldon, P.; Andriessen, R. Synthesis of malachite nanoparticles and their evolution during transmission electron microscopy. *J. Colloid Interface Sci.* **2008**, *323* (2), 282−285.
(31) Chen, J.-F.; Ding, H.-M.; Wang, J.-X.; Shao, L. Preparation and characterization of porous hollow silica nanoparticles for drug delivery application. *Biomaterials* **2004**, *25* (4), 723−727.
(32) Iftikhar, A.; Khan, M. S.; Rashid, U.; Mahmood, Q.; Zafar, H.; Bilal, M.; Riaz, N. Influence of metallic species for efficient photocatalytic water disinfection: Bactericidal mechanism of in vitro results using docking simulation. *Environ. Sci. Pollut. Res.* **2020**, *27* (32), 39819−39831.
(33) Riaz, N.; Hassan, M.; Siddique, M.; Mahmood, Q.; Farooq, U.; Sarwar, R.; Khan, M. S. Photocatalytic degradation and kinetic modeling of azo dye using bimetallic photocatalysts: effect of synthesis and operational parameters. *Environ. Sci. Pollut. Res.* **2020**, *27* (3), 2992−3006.
(34) Del Real-Olvera, J.; Morales-Rivera, J.; González-López, A. P.; Sulbarán-Rangel, B.; Zúñiga-Grajeda, V. Adsorption of Organic Pollutants from Cold Meat Industry Wastewater by Electrochemical Coagulation: Application of Artificial Neural Networks. *Water* **2020**, *12* (11), 3040.
(35) Maryanti, R.; Nandiyanto, A. B. D.; Manullang, T. I. B.; Hufad, A.; Sunardi, S. Adsorption of dye on carbon microparticles: physicochemical properties during adsorption, adsorption isotherm and education for students with special needs. *Sains Malays.* **2020**, *49* (12), 2977−2988.
(36) Önal, E. S.; Yatkın, T.; Aslanov, T.; Ergüt, M.; Özer, A. Biosynthesis and characterization of iron nanoparticles for effective adsorption of Cr (VI). *Int. J. Chem. Eng.* **2019**, *2019*, 1−13.
(37) Freundlich, H. Over the adsorption in solution. *J. Phys. Chem.* **1906**, *57* (385471), 385−471.
(38) Qiu, X.; Wang, S.; Miao, S.; Suo, H.; Xu, H.; Hu, Y. Co-immobilization of laccase and ABTS onto amino-functionalized ionic liquid-modified magnetic chitosan nanoparticles for pollutants removal. *J. Hazard. Mater.* **2021**, *401*, 123353.
(39) Farmany, A.; Mortazavi, S. S.; Mahdavi, H. Ultrasond-assisted synthesis of Fe_3O_4/SiO_2 core/shell with enhanced adsorption capacity for diazinon removal. *J. Magn. Magn. Mater.* **2016**, *416*, 75−80.
(40) Choi, K.-H.; Min, J.; Park, S.-Y.; Park, B. J.; Jung, J.-S. Enhanced photocatalytic degradation of tri-chlorophenol by Fe_3O_4@ TiO_2@Au photocatalyst under visible-light. *Ceram. Int.* **2019**, *45* (7), 9477−9482.
(41) Shilpa, G.; Kumar, P. M.; Deepthi, P. R.; Sukhdev, A.; Bhaskar, P.; Kumar, D. K. Improved Photocatalytic Performance of Fe_3O_4/ TiO_2 Thin Film in the Degradation of MB Dye Under Sunlight Radiation. *Braz. J. Phys.* **2023**, *53* (2), 38.
(42) Sarwar, A.; Wang, J.; Khan, M. S.; Farooq, U.; Riaz, N.; Nazir, A.; Mahmood, Q.; Hashem, A.; Al-Arjani, A.-B. F.; Alqarawi, A. A.; Abd_Allah, E. F. Iron Oxide (Fe_3O_4)-Supported SiO_2 Magnetic Nanocomposites for Efficient Adsorption of Fluoride from Drinking Water: Synthesis, Characterization, and Adsorption Isotherm Analysis. *Water* **2021**, *13* (11), 1514.
(43) Qin, H.; Tao, Y.; Niu, R.; Han, B.; Qiao, L. Flower-like mesoporous Fe_3O_4@SiO_2@F/NiO composites for magnetic solid-phase extraction of imidazole fungicides in tap water, milk and green tea. *Microchem. J.* **2023**, *185*, 108292.
(44) Tanaka, H.; Yamane, M. Preparation and thermal analysis of synthetic malachite CuCO 3· Cu $(OH)_2$. *J. Therm. Anal.* **1992**, *38* (4), 627−633.
(45) Saikia, J.; Saha, B.; Das, G. Efficient removal of chromate and arsenate from individual and mixed system by malachite nanoparticles. *J. Hazard Mater.* **2011**, *186* (1), 575−582.
(46) Geetha, P.; Latha, M.; Koshy, M. Biosorption of malachite green dye from aqueous solution by calcium alginate nanoparticles: equilibrium study. *J. Mol. Liq.* **2015**, *212*, 723−730.
(47) Gao, J.; Yuan, X. Vibrational Investigation of Pressure-Induced Phase Transitions of Hydroxycarbonate Malachite Cu_2 $(CO_3)(OH)$ $_2$. *Minerals* **2020**, *10* (3), 277.
(48) Nithya, R.; Thirunavukkarasu, A.; Sathya, A. B.; Sivashankar, R. Magnetic materials and magnetic separation of dyes from aqueous solutions: a review. *Environ. Chem. Lett.* **2021**, *19*, 1275−1294.
(49) Zangiabadi, M.; Shamspur, T.; Saljooqi, A.; Mostafavi, A. Evaluating the efficiency of the GO-Fe_3O_4/TiO_2 mesoporous photocatalyst for degradation of chlorpyrifos pesticide under visible light irradiation. *Appl. Organomet. Chem.* **2019**, *33* (5), No. e4813.
(50) Affam, A. C.; Chaudhuri, M. Degradation of pesticides chlorpyrifos, cypermethrin and chlorothalonil in aqueous solution by TiO2 photocatalysis. *J. Environ. Manage.* **2013**, *130* (0), 160−165.
(51) Marugán, J.; López-Muñoz, M. J.; Gernjak, W.; Malato, S. Fe/ TiO_2/pH Interactions in Solar Degradation of Imidacloprid with TiO_2/SiO_2 Photocatalysts at Pilot-Plant Scale. *Ind. Eng. Chem. Res.* **2006**, *45* (26), 8900−8908.
(52) Jaafari, J.; Barzanouni, H.; Mazloomi, S.; Amir Abadi Farahani, N.; Sharafi, K.; Soleimani, P.; Haghighat, G. A. Effective adsorptive removal of reactive dyes by magnetic chitosan nanoparticles: kinetic, isothermal studies and response surface methodology. *Int. J. Biol. Macromol.* **2020**, *164*, 344−355.
(53) Essandoh, M.; Garcia, R. A. Efficient removal of dyes from aqueous solutions using a novel hemoglobin/iron oxide composite. *Chemosphere* **2018**, *206*, 502−512.
(54) Beigi, P.; Ganjali, F.; Hassanzadeh-Afruzi, F.; Salehi, M. M.; Maleki, A. Enhancement of adsorption efficiency of crystal violet and chlorpyrifos onto pectin hydrogel@Fe_3O_4-bentonite as a versatile nanoadsorbent. *Sci. Rep.* **2023**, *13* (1), 10764.
(55) Ohale, P. E.; Igwegbe, C. A.; Iwuozor, K. O.; Emenike, E. C.; Obi, C. C.; Białowiec, A. A review of the adsorption method for norfloxacin reduction from aqueous media. *MethodsX* **2023**, *10*, 102180.
(56) Ghanbari, N.; Ghafuri, H. Preparation of novel Zn-Al layered double hydroxide composite as adsorbent for removal of organophosphorus insecticides from water. *Sci. Rep.* **2023**, *13* (1), 10215.
(57) Beyki, M. H.; Shemirani, F.; Malakootikhah, J.; Minaeian, S.; Khani, R. Catalytic synthesis of graphene-like polyaniline derivative - MFe_2O_4 (M; Cu, Mn) nanohybrid as multifunctionality water decontaminant. *React. Funct. Polym.* **2018**, *125*, 108−117.

https://doi.org/10.1021/acsomega.3c08419
ACS Omega 2024, 9, 13803−13817